

CLIPGen: A Chiplet Link IP Modeling and Generation Framework for 2.5D Architecture Exploration

Zhengping Zhu
zz2168@nyu.edu
New York University
Brooklyn, New York, USA

Austin Rovinski
rovinski@nyu.edu
New York University
Brooklyn, New York, USA

Abstract

Advanced 2.5D Systems-in-Package (SiPs) compose a growing portion of high-performance systems. While the packaging and interconnect choices play a large role in the overall system design, system architects still lack a suitable framework for early design space exploration which takes these choices into account. Current interconnect models fall mostly into the categories of 1) detailed models which are generally inflexible and require deep packaging expertise, or 2) high-level models which don't provide enough information to make accurate architectural design decisions.

In this work, we present an automated chiplet IP generation framework which provides power, performance, and area estimates for various 2.5D packaging and communication configurations. The IP generator produces standard collaterals required for high-level simulation/estimation, RTL simulation, and place-and-route-level implementation (Verilog, Liberty, LEF, and datasheet). Using our framework, architects can co-optimize the package and chiplet architecture through rapid power, performance, and area estimates of various packaging strategies. As a case study, we examine generated UCIE interfaces across several packaging options.

Keywords

2.5D, IP, Die-to-die link modeling

1 Introduction

Chiplet-based systems have taken hold as a prime technology to enable continued scaling of computational systems beyond the end of Moore's Law. Chiplets offer several advantages over monolithic chips, including expanding logic beyond the die reticle limit, increasing yields above comparably sized monolithic systems, and increasing composability of systems by mixing/matching different chiplets during assembly.

However, system architects face significant challenges in performing design space exploration with different chiplet configurations to determine power, performance, and area (PPA) tradeoffs. Many prior works focus on either high-level modeling, which don't provide sufficient detail to make design decisions [1, 13, 18, 20], or extremely deep modeling [22], which requires significant packaging expertise and effort from the architect. Both ends of the spectrum often focus on a single technology stack, which significantly limits the design space when multiple packaging and process technologies are available at varying costs.

In this work, we present CLIPGen, a 2.5D chiplet I/O modeling framework and IP generator. The CLIPGen flow is shown in Fig. 1. CLIPGen takes in standard process design kit (PDK) files and a simple configuration file from the user as input. As output, it generates IP collaterals necessary for design space exploration at the pre-RTL,

post-synthesis, and post-routing stages. CLIPGen automatically generates datasheet (.txt), Verilog (.v), Liberty (.lib), physical abstract (.lef), and SPICE (.scs) formats. CLIPGen also generates a design constraint file (.sdc) which can be used to properly model interface constraints.

In addition, users with packaging and interconnect expertise can modify default model parameters (such as the degree of electrostatic discharge (ESD) protection) or even override internal parameters of the model to perform theoretical "what if?" exploration (such as the amount of coupling capacitance between channels).

This work bridges the gap not filled by existing frameworks – we offer a multi-technology, multi-package I/O and link modeling framework which can offer accurate PPA metrics with negligible expertise from computer architects. In this work, we offer the following contributions:

- A chiplet link modeling framework which generates collaterals suitable for both early-stage and detailed PPA analysis, including datasheet, Verilog, Liberty, LEF, SPICE, and SDC
- A set of default, realistic packaging configurations to support system-level modeling and sweeps without requiring detailed packaging expertise.
- A detailed configuration framework which allows overriding modeling parameters and "what if?" exploration
- A case study of a UCIE interconnect across various packaging and technology configurations, demonstrating the importance of properly modeling interconnects at the architectural level.

2 Related Works

Prior modeling work in 2.5D chiplet I/O and link can be broadly classified into 3 categories: 1) Fabricated, lab-characterized chiplets, 2) Implementation-specific, detailed models, and 3) High-level modeling frameworks.

2.1 Fabricated Chiplets

Many prior works have explored chiplet interconnects and reported measurements for their systems [6, 8, 9, 11, 16]. Using these reported real measurements is enticing for architects, as it anchors their estimation in a ground truth. However, these works pose several issues for use in estimating PPA. While there is a large body of work exploring more traditional 2D links (e.g. link length >40mm [16]), many fewer works report results in the 2.5D regime (link length <10mm [8, 11]). These works often report metrics piecemeal, with measurements such as I/O power remaining a single value and not breaking it down between components (TX, RX, link, protocol logic, etc.), or omit critical packaging details for contextualizing results.

Automated Chiptlet D2D Link Generation Framework

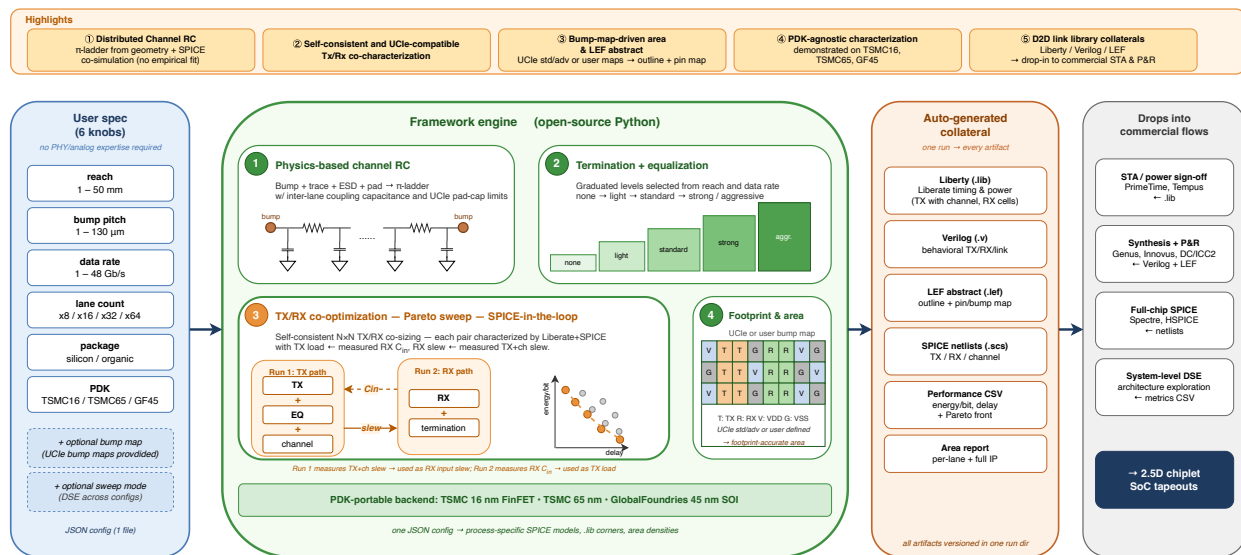


Figure 1: Overview of the proposed automated chiptlet D2D link generation framework. A single JSON specification (reach, bump pitch, data rate, lane count, package type, PDK) drives: (1) a π -ladder channel RC derived from bump/trace/pad geometry and co-simulated in Liberate; (2) reach- and data-rate-driven auto-selection of termination and passive equalization; (3) self-consistent TX/RX co-characterization over an $N \times N$ sizing grid, realized as two Liberate+SPICE runs that exchange measured RX C_{in} and TX+channel slew, with a Pareto front filtered under the UCIE latency bound; and (4) bump-map-driven area estimation and LEF abstract generation (UCIE standard/advanced or user-supplied maps). The resulting .lib, Verilog, and LEF are drop-in for commercial STA and P&R tools. The flow is PDK-agnostic and demonstrated on TSMC 16 nm FinFET, TSMC 65 nm, and GF 45 nm SOI.

Beyond missing data, characterized chiptlets are also *inflexible*, as they offer data for one very specific design point and don't offer insight for nearby design points. The data may also be subtly incompatible with the prototype system, due to a mismatch in process nodes (e.g. a 3nm IP on a 12nm chip) or other incompatibilities.

Our framework addresses this inflexibility by supporting arbitrary process nodes and a wide range of packaging options. All configuration options and metrics are reported to the user, and CLIPGen is calibrated against real works to present realistic data.

2.2 Detailed Models

An alternative approach to real-chiptlet data is to use highly detailed models of chiptlet interconnects. Some works propose using schematic-based models which may include lumped or distributed parasitics models [12, 22]. While these works can offer high accuracy through detailed models, these models have cumbersome interfaces which require significant packaging expertise to understand. For example, a user may need to *manually* supply bump, pad, and trace capacitances, and these values need to be accurate to receive reasonable results from the model. Architects are often not concerned with this level of detail, and may worry about receiving unrealistic results from a miscalibrated model. Further, these models provide mainly the channel model and possibly a driver model.

To the best of our knowledge, they do not model other commonly required high-speed I/O components such as ESD protection, equalizers, and termination, all of which impact the PPA of the chiptlet link.

Our framework addresses this complication by providing simple, high-level parameters and reasonable default options for architects to use. The framework sources its internal properties from well-established physical constants (material permittivities, resistivity, trace parasitics per unit length), while still allowing users to override any parameters and provide their own values for calibration.

2.3 High-level Models

High-level modeling refers to models which use either static, fixed values, or very simple knobs to provide rapid estimates with minimal configuration. High-level models are typically preferred by computer architects as they don't require expertise to configure or add to their system-level model. Many prior works simply use bandwidth numbers reported from prior works or specifications [2]. These works suffer from either lack of accuracy (especially relative to the I/O vs. logic), or lack of information, where the work may simply not account for or report important metrics like power and area [1, 13, 18, 20].

Other times, works may select a single data point from a real chiplet system or detailed modeling framework [5], which neglects any benefits of design space exploration. Further, the selected data point may differ in technology from other simulated results in the paper.

2.4 Other Chiplet Models

Several works have explored modeling other properties of 2.5D chiplets, such as cost and yield [4, 7] and thermal properties [15, 23]. These works are orthogonal to this work, as they do not focus on the overall PPA modeling of chiplet interfaces. Many works also focus on 3D chiplet integration. While 3D integration is extremely promising for high performance interconnects, we focus on 2.5D modeling because 3D integration still faces steep challenges from thermal dissipation and yield. Additionally, interconnects in 3D systems generally are short enough (<150um) that they are firmly in the RC modeling regime and can be modeled fairly accurately as long on-chip wires.

3 CLIPGen Framework

CLIPGen follows four core design principles: (1) **directional accuracy**—capture trends under parameter sweeps; (2) **relative accuracy**—provide fair PPA comparison of I/O vs. logic; (3) **ease of use**—provide realistic estimates without interconnect expertise or excessive runtime; (4) **flexibility**—support multiple PDKs and parameter overrides. Rather than aiming for tapeout-ready IP, CLIPGen captures realistic PPA into standard EDA collateral (Liberty, Verilog, LEF) suitable for system-level exploration with existing digital tools.

CLIPGen accepts a single JSON configuration file and produces a complete set of standard EDA collateral—Liberty timing/power models, synthesizable Verilog, LEF physical abstractions, and a metrics datasheet—for a parameterized chiplet die-to-die (D2D) link IP. The framework supports two operating modes: (1) *single-point* mode, which generates and characterizes one link configuration and optionally runs joint TX/RX co-optimization; and (2) *sweep* mode, which evaluates a user-defined Cartesian product of link parameters in parallel, producing a multi-dimensional design-space dataset with a single invocation.

The end-to-end pipeline is illustrated in Fig. 1. Starting from a physical channel RC model, the framework proceeds through automated link adaptation (termination and equalization), transceiver circuit sizing, SPICE-level characterization via Cadence Liberate, and finally collateral generation. Each stage feeds the next: channel parasitics set the characterization load for the TX Liberty run; the TX output slew in turn sets the RX characterization index; and the resulting Liberty timing arcs compose the full-link delay and energy budget reported in the datasheet.

3.1 Configuration Interface

A deliberate two-tier parameter hierarchy separates *user-facing* parameters from *hidden* physical constants. User-facing parameters describe the target link in terms an architect naturally controls: package type, reach, bump pitch, data rate, lane count, and high-level design-intent flags (Table 1). These are the only fields that must be set to explore a new configuration.

Hidden parameters (JSON sections suffixed `_hidden`) encode literature-sourced physical constants—dielectric permittivities, bump resistivity, trace RC per unit length, and PHY boundary tables—that are fixed for a given package technology. Expert users may override them when calibrating the model to measured data, but they need not be touched for ordinary design-space exploration. This separation removes the requirement for packaging expertise to operate the framework at the architect level.

Table 1: User-facing configuration parameters.

Parameter	Type	Description
<code>pkg_type</code>	si org	Package / interposer technology
<code>reach_mm</code>	float	Die-to-die interconnect length
<code>bump_pitch_um</code>	float	Bump-to-bump pitch
<code>data_rate_Gbps</code>	float	Per-lane NRZ data rate
<code>lane_count</code>	int	Number of D2D lanes
<code>passive_eq_en</code>	bool	Enable passive TX pre-emphasis
<code>ac_coupled</code>	bool	Enable AC-coupled RX termination
<code>pad_cap_mode</code>	phys ucie	Geometry model or UCIE spec

3.2 Operating Modes and Options

Beyond the eight core link parameters, CLIPGen exposes a rich set of operating modes that control channel modeling fidelity, transceiver sizing strategy, characterization accuracy, physical layout, and output artifacts. All modes have reasonable defaults so that a minimal config runs end-to-end without modification; users selectively enable or tune options as their exploration matures.

Channel fidelity options. The pad capacitance model is switchable between a geometry-derived parallel-plate model (`pad_cap_mode: physical`) and a UCIE Standard Package specification lookup table (`pad_cap_mode: ucie`), which returns the spec-mandated maximum pad cap (300/200/125 fF) for the configured data rate. The `ucie` mode is useful for compliance-centric analysis where the pad cap budget is fixed by the standard rather than the physical geometry; it also subsumes ESD capacitance, which the physical model tracks separately.

Inter-lane coupling capacitance can be enabled or disabled as a block (`coupling_cap.enabled`). When enabled, three knobs are exposed: `cc_ratio_trace` (coupling fraction at each trace Pi-ladder node, typically 0.3–0.5 for edge-coupled microstrip), `cc_ratio_pad` (fraction at interposer pad nodes, smaller since pads are more widely spaced than traces), and `cc_rx_pad_ff` (absolute on-die RX pad-to-pad fringe capacitance in fF). The coupling elements are injected directly into the SPICE netlist so that Liberate captures their effect on TX output transition time and RX input sensitivity.

Geometric channel parameters—bump diameter, bump height, trace width, and ESD type—all default to package-derived values but may be overridden individually when the physical design deviates from the default rules.

Transceiver sizing hierarchy. CLIPGen offers four progressively more powerful sizing strategies, summarized in Table 2. Users start with the simplest mode that meets their needs and escalate as the design matures.

The `co_opt` mode additionally exposes `n_tx_configs` and `n_rx_configs` (number of configurations in the exploration grid), `max_`

Table 2: Transceiver sizing modes, in order of increasing automation.

Mode	Description	Best for
Manual	User specifies TX and RX transistor widths directly	Porting a known design
tx_sizing	Adaptive SPICE search (golden-section) to meet UCIE rise/fall target (<code>rise_fall_pct_ui</code>) within a simulation budget	TX-only tuning
rx_sizing	Iterative RX width search to satisfy a maximum RX delay fraction of UI	RX-only tuning
co_opt	Joint TX+RX Pareto optimization via LUT matching; supercedes the two modes above	Full link optimization

parallel (concurrent characterization processes), and pareto_selection (balanced, best_power, best_delay, or all to return the full frontier).

Characterization options. The standard mode embeds the channel RC π -ladder inside the TX SPICE subcircuit, so Liberate characterizes the full TX+channel path in one run, producing a single timing arc that captures channel loading inherently. (A legacy false option exists for external analytical correction, but is non-standard.) The `rx_slew_source` option selects whether RX input slews are drawn from the TX pad before the channel (`tx_pad`) or from the far end of the π -ladder (`channel`); the latter is physically correct. An explicit `input_slews_ns_override` list may override auto-detection if needed.

Physical layout mode. When `bump_map_enabled` is set, CLIP-Gen reads a user-supplied bump map text file that assigns each bump site to a role: tx, rx, vdd, vss, other, or empty. The bump count for tx and rx roles must match `lane_count`; power and ground bump counts are free. The area model and LEF generator use the bump map to produce a full-footprint macro bounding box with correct pin placement for each role, enabling accurate floorplan integration. Without a bump map, only per-lane area is reported.

Output control. Each output artifact is independently toggled: SPICE netlists (`save_netlists`), Liberate characterization scripts (`save_liberate_decks`), Liberty files (`save_lib`), aggregate metrics CSV (`save_metrics_csv`), Verilog (`generate_verilog`), and LEF (`generate_lef`). This allows, for example, a sweep run to save only the CSV for rapid analysis while suppressing the larger binary and netlist artifacts.

3.3 Physical Channel Model

Full-wave electromagnetic (EM) tools can model 2.5D interconnects with high accuracy but require hours per configuration, unsuitable for design-space exploration. For the UCIE Standard regime (≤ 32 Gbps, ≤ 50 mm), the electrical length is well under one-tenth the signal wavelength at Nyquist; RC parasitics dominate the signal integrity mechanism, with sufficient accuracy for this design space [3]. Inductive effects are negligible; skin-effect-corrected bump resistance is used.

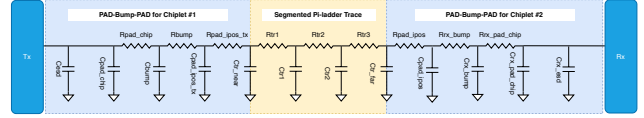


Figure 2: Distributed π -ladder channel model. Per-element R+C for chiplet and interposer pads, microbumps, and ESD shunt caps at each chiplet side; three-segment π -ladder for the trace (near half-cell, three series resistors with shunt caps, far half-cell).

The channel model computes per-segment RC values for each 2.5D component: chiplet pad, microbump, interposer pad, trace (three segments), and ESD protection. These values are assembled into a distributed π -ladder SPICE subcircuit (`txip.scs`) and embedded directly in the TX characterization netlist, so Liberate produces timing arcs that include channel propagation without external analytical correction. The same per-segment RC values also support rapid Elmore-based pre-filtering during design-space exploration. All components are parameterized by user-facing geometry (bump pitch, reach) together with package-type-dependent constants from the hidden config.

Per-component models. All physical constants (material permittivities, resistivity, trace parasitics, interposer layer thicknesses, ESD targets) are sourced from literature [3, 10, 17, 19, 21], ensuring calibration against industry-standard references and enabling multi-technology portability.

Pad capacitance is modeled as a parallel-plate capacitor scaled by pad width $w_p = 0.8 \cdot P$ (bump pitch P) and ILD thickness t_{ox} :

$$C_{\text{pad}} = \epsilon_0 \epsilon_r \frac{w_p^2}{t_{ox}}. \quad (1)$$

Pad resistance scales inversely with w_p from a reference measurement. Bump capacitance uses a two-wire cylindrical model with underfill permittivity; bump resistance accounts for both DC and skin-effect (AC) contributions at the Nyquist frequency $f_{Ny} = R_b/2$:

$$R_{\text{bump}} = \sqrt{R_{DC}^2 + R_{AC}^2}. \quad (2)$$

Trace capacitance and resistance are scaled from tabulated base values (silicon interposer: 185 fF/mm, 1.04 Ω /mm at 3 μm width; organic substrate: 138 fF/mm, 0.036 Ω /mm at 30 μm width [3]) by width and dielectric ratio. ESD capacitance is selected from a graduated table keyed on bump pitch and package type, reflecting CDM target-level specifications [17].

SPICE simulation. The per-segment RC values are assembled into a three-segment π -ladder SPICE subcircuit embedded in `txip.scs`, which Liberate co-characterizes with the TX driver at each configuration point. This produces Liberty timing arcs that intrinsically capture the channel's effect on TX slew and delay, with no external analytical correction needed.

Analytical filtering (optional). For rapid Pareto pre-filtering during design-space sweeps, a lumped Elmore reduction over the same RC values provides sub-millisecond estimates of delay and

energy:

$$\tau_{\text{Elmore}} = R_{ch} \cdot C_{ch}, \quad (3)$$

$$E_{ch} = \frac{1}{2} C_{\text{eff}} V_{DD}^2, \quad (4)$$

where C_{eff} counts the chiplet pad, microbump, and interposer pad twice each (charged and discharged per bit) and single-counts the trace and ESD. This analytical estimate pre-filters the design space; final timing and energy metrics come from the full SPICE π -ladder via Liberty.

Configuration options. An alternative *UCIe pad cap mode* replaces the geometry-derived pad capacitance with the UCIe Standard Package specification lookup table (300 fF at ≤ 8 GT/s; 200 fF at ≤ 16 GT/s; 125 fF at ≤ 32 GT/s), absorbing ESD into the spec budget. Inter-lane coupling capacitance can be enabled as a ratio of per-node shunt capacitance, injected into the SPICE π -ladder as coupling elements between adjacent lanes.

3.4 Automated Link Adaptation

Given the computed channel RC, CLIPGen automatically determines whether termination and equalization are needed and sizes their components from first-principles models. The user only sets high-level flags (`passive_eq_enabled`, `ac_coupled`); all thresholds and values are computed by the framework.

Termination. For short-reach links within the UCIe unterminated operating boundary, impedance matching is unnecessary and termination adds power overhead without SI benefit. Beyond the boundary, reflection suppression is required. The Thevenin-split topology (two high-impedance bias resistors to mid-rail, plus termination resistor R_T) is UCIe-specified and avoids DC bias current, keeping static power negligible [2]. Rather than binary on/off, CLIPGen uses a graduated four-level scheme: as reach exceeds the unterminated boundary, stronger termination (lower R_T) is selected progressively, matching overhead to actual SI need. The need and level are decided by a UCIe-based boundary table indexed by TX swing and data rate, yielding the maximum unterminated reach L_{unterm} . The reach ratio $\rho = L/L_{\text{unterm}}$ selects one of four graduated levels:

Table 3: Graduated termination levels.

Level	ρ range	R_{term}	C_{AC}
0 – none	≤ 1.0	—	—
1 – light	≤ 1.25	$2R_{RX}$	$0.5C_{base}$
2 – standard	≤ 1.5	R_{RX}	C_{base}
3 – strong	> 1.5	$0.5R_{RX}$	$2C_{base}$

The Thevenin-split topology sets $V_{\text{TERM}} = V_{DD}/2$ via high-impedance bias resistors (1 M Ω), keeping static bias current negligible. Termination energy per bit combines the static bias dissipation and the dynamic switching component through R_{term} .

Equalization. Active equalization (FFE) requires a DAC, multi-tap serializer, and significant power/area overhead. For short-reach, moderate-loss channels (dominant degradation: first-order RC roll-off, not multi-pole), a single-zero passive equalizer suffices: a series poly-R and shunt MIM/MOM-C at the TX output create a high-pass response that cancels the RC roll-off with only two passive

components. Like termination, equalizer strength is graduated (five levels: none through aggressive) and auto-selected based on channel loss. Short, low-loss links engage no EQ; longer/higher-rate links engage progressively stronger pre-emphasis, avoiding unnecessary area on links that don’t need it.

The channel RC low-pass loss at Nyquist,

$$\text{Loss}_{Ny} = 10 \log_{10} \left[1 + \left(\frac{f_{Ny}}{f_{3dB}} \right)^2 \right], \quad (5)$$

is compared against a configurable threshold to select one of five graduated passive EQ levels (*none* through *aggressive*). The selected level maps to an equalizer capacitance fraction α of C_{ch} , where

$$\alpha \in \{0, 0.05, 0.10, 0.15, 0.20\}.$$

Component values are derived by placing the EQ zero at the channel –3 dB corner:

$$C_{eq} = \alpha C_{ch}, \quad R_{eq} = \frac{R_{ch}}{\alpha}. \quad (6)$$

R_{eq} is additionally capped so that $R_{eq} \cdot C_{\text{downstream}}$ does not exceed a latency budget multiple of the unit interval, preventing excessive pre-emphasis on long-reach channels.

3.5 Transceiver Sizing and Characterization

TX Architecture. For short-reach D2D links at UCIe Standard data rates and bump pitches, pad capacitance is modest (125–300 fF) and signal swing is full-rail CMOS. A tapered CMOS inverter chain is the dominant TX architecture in published designs [2]: lowest static power (no DC bias), simplest analytical sizing, direct Liberty compatibility. (High-swing differential topologies offer better SI at longer reaches but incur static power and different termination strategy; they are outside the current Standard Package scope.)

The chain fanout factor is sized analytically following geometric progression $f \approx e \approx 2.718$ (adjusted for parasitic capacitance), with stage count forced even to maintain non-inverting polarity at the pad. A SPICE Q/V simulation measures the unit inverter input capacitance; the full chain is then sized geometrically. When passive EQ is enabled, the computed R_{eq} and C_{eq} are patched into the TX netlist template. The channel RC π -ladder is embedded directly in the TX subcircuit so that a single Liberate run characterizes the full TX+channel path.

RX Architecture. The RX faces two competing constraints: minimize input capacitance seen by the channel (preserve bandwidth), yet drive core logic fanout. A single inverter cannot do both; a two-stage topology resolves this: small pre-amplifier (minimal input cap) + larger output buffer (core fanout). This standard short-reach RX architecture [2, 3] maps naturally to a two-cell Liberty abstraction with separate input/output characterization points.

Input slew for RX characterization is auto-detected from the TX output waveform at the far end of the channel π -ladder, ensuring consistent characterization conditions without manual input specification. An optional sizing mode iterates buffer widths to satisfy a maximum RX delay fraction of the unit interval.

Area model. The silicon footprint of each TX and RX IP macro is computed analytically from the sized component values, using process-specific density constants from the `area_hidden` config section: active transistor area (with a layout margin factor for contacts, poly extensions, and well taps), passive EQ (poly-R strip and

MIM/MOM capacitor), termination bias resistors, and ESD diode area derived from pad capacitance. Bump and UBM pad geometry follows assembly-regime rules: Cu pillar/C4 for pitch $P \geq 10 \mu\text{m}$, hybrid bonding (Cu–Cu direct bond, no UBM overhang) for $P < 10 \mu\text{m}$. The bounding box dimensions feed directly into the LEF macro generator.

3.6 TX/RX Co-Optimization via Pareto Search

TX and RX sizing are mutually coupled: TX delay and output slew depend on the RX input capacitance (output load), while RX delay depends on the TX output slew (input transition time). Sizing each independently ignores this coupling and produces suboptimal results. CLIPGen formulates the joint optimization as a multi-objective problem over the Pareto frontier of total energy per bit and worst-case link latency.

Lookup-table matching. Rather than running a Liberate characterization for every $(\text{TX}_i, \text{RX}_j)$ pair, CLIPGen exploits the separability of the characterization tables. Each TX configuration is characterized *once* with a sweep of output loads covering the full RX input capacitance range; each RX configuration is characterized *once* with a sweep of input slews covering the full TX output slew range. For each pair, metrics are obtained in sub-millisecond time by interpolation:

- (1) Read RX_j input capacitance C_{RX} from its Liberty attribute.
- (2) Interpolate TX_i tables at load = $C_{RX} \rightarrow$ TX delay, output slew, switching power.
- (3) Interpolate RX_j tables at input slew = TX_i output slew \rightarrow RX delay, switching power.
- (4) Sum delay; compute total $E/\text{bit} = \alpha(E_{TX} + E_{RX}) + E_{ch} + E_{term}$.

Total Liberate invocations: $N_{TX} + N_{RX}$, versus $O(N_{TX} \times N_{RX})$ for a brute-force grid.

Pareto frontier. The feasible set (configurations satisfying the UCIe latency constraint) is reduced to a non-dominated frontier on $(E_{\text{total}} [\text{pJ}/\text{bit}], \tau_{\text{wc}} [\text{ps}])$, where $\tau_{\text{wc}} = \max(\tau_{RR}, \tau_{FF})$ is the worst-case TX+channel+RX delay. Three automated selection strategies are provided: balanced (minimum Euclidean distance to the ideal point), best_power, and best_delay.

3.7 Multi-PDK Portability

CLIPGen provides production-quality configurations for three process nodes: TSMC 65 nm planar CMOS, TSMC 16 nm FinFET, and GF 45 nm SOI. Process-specific differences are fully encapsulated within each config file and the corresponding Liberate characterization template (SPICE netlist, characterization script): FinFET fin-count quantization (e.g., $w = 0.01 + 0.048(n_{fin} - 1) \mu\text{m}$), MIM vs. MOM capacitor density, BEOL ILD thickness, and supply voltage scaling are all handled automatically. The analytical models (channel, equalization, termination, area) are process-agnostic and require no modification when switching nodes.

Porting to a new process node requires authoring a JSON config and a Liberate netlist template. The JSON config supplies transistor names, minimum/maximum widths, PDK model file path, and process corner; the template provides a unit TX inverter subcircuit that the framework wraps into the multi-lane txip netlist and patches with the computed EQ and termination parameters.

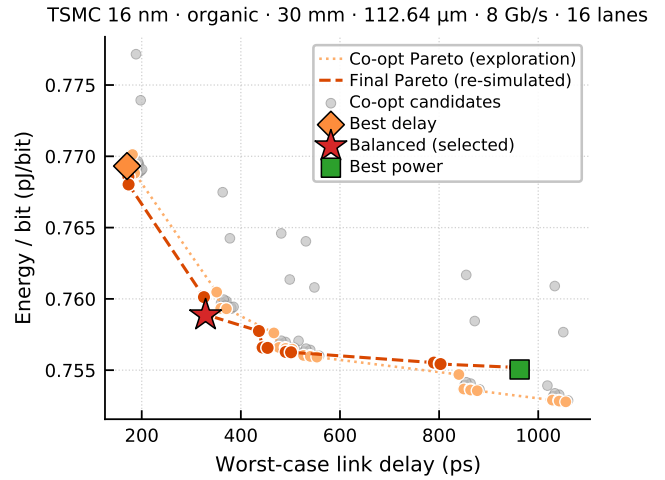


Figure 3: Energy-per-bit vs. worst-case link delay for a 16-lane UCIe Standard link (TSMC 16 nm, organic substrate, 112.64 μm bump pitch, 8 Gb/s, 30 mm reach). Grey dots are all TX/RX sizing candidates examined during co-optimization. The light-orange dotted curve is the Pareto frontier estimated during the exploration phase; the dark-orange dashed curve is the frontier after the final re-characterization with matched TX output slew and RX input capacitance. Three representative operating points are highlighted: minimum-delay (orange diamond), balanced energy–delay knee (red star, auto-selected), and minimum-energy (green square).

3.8 Design Space Exploration and Collateral Generation

In sweep mode, CLIPGen evaluates the full Cartesian product of $\{\text{pkg_type}\} \times \{\text{reach_mm}\} \times \{\text{bump_pitch_um}\} \times \{\text{data_rate_Gbps}\}$ in parallel, limited by a configurable worker count. Each point independently traverses the full pipeline—channel model, adaptation, characterization, co-optimization—and writes its results to a per-configuration subdirectory. An aggregate CSV collects all metrics, enabling cross-sweep Pareto analysis and visualization (e.g., energy vs. reach across package technologies, EQ/termination regime maps).

For every evaluated configuration, CLIPGen produces the following standard collateral:

- **Liberty (.lib):** NLDM timing and internal switching power for txip and rxip, compatible with Synopsys PrimeTime and open-source OpenSTA.
- **Verilog:** Behavioral RTL model with correct port naming and bus widths for lane_count lanes, suitable for RTL-level simulation.
- **LEF:** Physical macro abstraction with pin locations derived from the bump map and area model bounding box, suitable for place-and-route floorplanning.
- **Datasheet / CSV:** Per-configuration PPA summary including per-lane and aggregate energy breakdown, latency, area, and the engaged termination and equalization levels.

4 Experiments and Results

4.1 Pareto-Guided Design-Point Selection

Figure 3 shows how CLIPGen converts a single link configuration into a family of Pareto-optimal design points. For the 30 mm organic UCIE Standard link at 8 Gb/s, the $N \times N$ co-optimization grid (Section 3.6) produces dozens of feasible TX/RX pairs (grey cloud) spanning more than $2\times$ in worst-case delay. The non-dominated subset forms the Pareto frontier; CLIPGen exposes three canonical selections (minimum delay, minimum energy, balanced knee) and emits the full frontier as collateral.

The two frontiers in Fig. 3 differ slightly because exploration approximates the per-stage TX load and RX input slew from shared lookup tables to keep the $N \times N$ sweep tractable, while the re-characterization step re-simulates each surviving pair with matched C_{in} and TX+channel slew. The shift is typically a few percent in energy and tens of picoseconds in delay, and the final curve is what populates the generated .lib, .lef, and Verilog collateral.

4.2 Short-Reach: When Does an Organic Substrate Beat a Silicon Interposer?

Conventional wisdom holds that a silicon interposer (UCIE Advanced, 25 μm pitch) is always superior to an organic substrate (UCIE Standard, 112.64 μm pitch) at short reach because of its lower bump capacitance. Figure 4 tests this on a single-lane 48 Gb/s link sweeping reach from 2 to 25 mm on both packages across the same three nodes, plotting only UCIE-feasible points.

Contrary to intuition, the two curves cross: for all three PDKs the best-power energy curves intersect near **10 mm**, and at 25 mm the gap exceeds $2\times$ in the organic’s favour (e.g. 0.41 vs. 0.83 pJ/bit on TSMC 16 nm; 0.63 vs. 1.76 pJ/bit on TSMC 65 nm). Silicon has a small delay edge only at 2–4.5 mm, after which its best-delay jumps to ~ 150 –200 ps while organic stays in the 50–120 ps range out to 25 mm.

The modeling flow (Section 3.3) explains the crossover via two opposing terms. *Bump/pad capacitance* (Eqs. (1)–(2)): the 112.64 μm organic bump costs ≈ 63 fJ/bit at the pad versus ≈ 4.5 fJ/bit for the 25 μm silicon bump—a fixed ~ 60 fJ/bit penalty organic always pays. *Distributed channel RC* (Section 3.3): the fine-pitch silicon wires have much higher resistance per mm, so the Elmore constant (3) degrades rapidly and the co-optimizer must drive the channel harder. On TSMC 16 nm best-power, silicon E_{TX} rises from 0.8 fJ/bit (2 mm) to 28 fJ/bit (9.5 mm), 234 fJ/bit (20 mm), and over 2 pJ/bit by 42.5 mm; organic stays in single-digit fJ/bit until ~ 30 mm. At ~ 10 mm the silicon TX blow-up has erased its bump-cap advantage, and for longer reach the thicker organic trace’s lower resistance dominates. This is exactly the package-level trade-off that is tedious to hand-calibrate but falls out naturally from the parameterized channel and TX/RX co-optimization in CLIPGen.

4.3 Cross-Node Reach Sweep at 48 Gb/s

We stress the generator across technology and physical-channel axes on a 16-lane UCIE Standard link (48 Gb/s/lane, 16-UI ≈ 333 ps budget) on three process nodes: TSMC 16 nm (0.8 V), TSMC 65 nm (1.0 V), and GF 45 nm. Reach is swept from 2 to 50 mm (2.5 mm grid up to 30 mm, calibrated to the ISSCC 2026 prototype [14]),

UCIE Standard vs. Advanced · Single Lane · 48 Gb/s

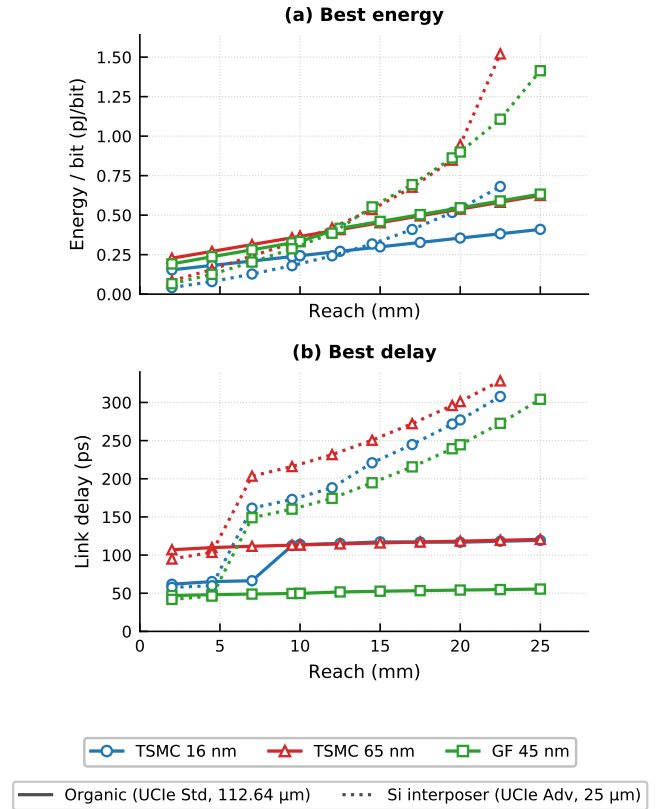


Figure 4: Single-lane, 48 Gb/s short-reach comparison of an organic UCIE Standard substrate (112.64 μm bump pitch, solid lines) and a silicon interposer (25 μm bump pitch, dotted lines) across three PDKs. (a) Energy per bit of the *best-power* Pareto selection. (b) Worst-case link delay of the *best-delay* Pareto selection. Only delay-feasible points under the UCIE 16 UI latency budget are plotted.

and 5 mm beyond. For every (node, reach) point the full flow from Section 3.6 is executed and the latency budget is applied as a hard feasibility filter. We report three frontier selections: *balanced* (knee), *best-power*, and *best-delay*.

Figure 5 shows that the three nodes separate cleanly. TSMC 16 nm delivers the lowest energy per bit (~ 0.77 pJ/bit at 30 mm vs. 1.2–1.4 pJ/bit elsewhere) because its 0.8 V supply gives a quadratic switching-energy advantage. GF 45 nm produces the lowest delay at every reach (~ 60 ps at 30 mm for best-delay vs. ~ 125 ps for TSMC 65 nm) thanks to faster devices, but at higher energy than TSMC 65 nm—it is the *fast* node rather than the *efficient* one.

The curve shapes also expose how the selector trades the two metrics. Best-power energy is nearly linear in reach because the selector spends latency slack freely up to the 333 ps ceiling; the corresponding delay trace (panel e) is therefore jagged. The best-delay column is the mirror image: smooth delay (panel f) and noisier energy (panel c). A step-up in delay near 30–35 mm appears across

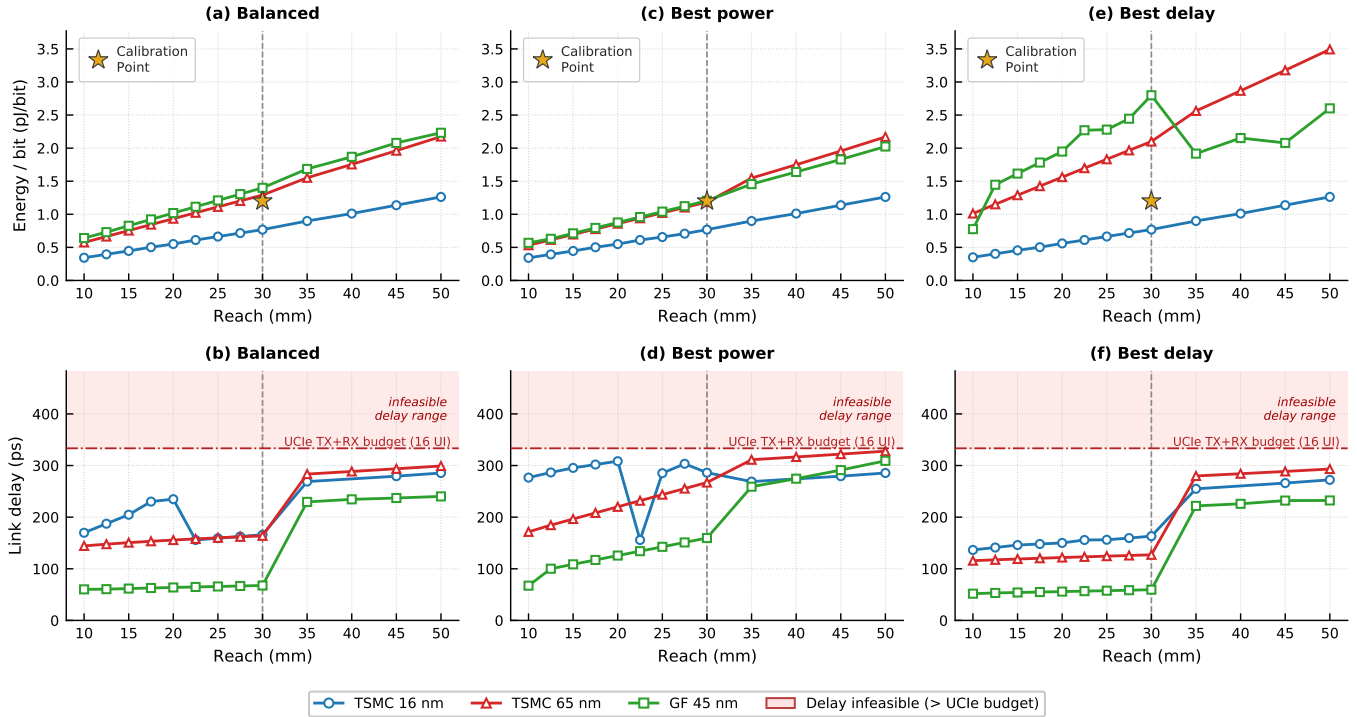


Figure 5: Modeled link energy per bit (top row) and worst-case link delay (bottom row) versus reach for a 16-lane chiplet link at 48 Gb/s on an organic UCIe Standard substrate (12-column \times 16 bump map, 112.64 μm bump pitch), swept across three process nodes: TSMC 16 nm (VDD = 0.8 V), TSMC 65 nm (VDD = 1.0 V), and GF 45 nm (VDD = 1.0 V). Columns correspond to three Pareto-optimal design-point selections: (a, d) balanced energy–delay trade-off, (b, e) minimum-energy (*best-power*), and (c, f) minimum-delay (*best-delay*). The red dash-dot line in the delay panels marks the UCIe TX+RX latency budget of 16 UI (\approx 333 ps at 48 Gb/s); the shaded band above it is the infeasible region. The vertical dashed line at 30 mm is the calibration reach, and the gold star on the energy panels marks the corresponding measured operating point from the ISSCC 2026 UCIe-compliant 48 Gb/s silicon prototype [14].

all selections: the organic channel is RC-limited and its Elmore constant grows super-linearly, so past \sim 30 mm the co-optimizer rebalances the driver (stage count is integer, producing a step rather than a ramp). E.g., at 35 mm the TSMC 16 nm best-power design doubles its stage count from 6 to 12; past this transition, the curves resume a smooth reach dependence.

5 Conclusion

We presented CLIPGen, an automated framework that embeds a distributed π -ladder channel RC model directly into SPICE characterization, producing Liberty timing arcs with intrinsic channel propagation delay. This bridges the gap between high-level approximations and detailed EM models, enabling rapid design-space exploration without packaging expertise.

The framework automates the full pipeline from JSON configuration to Liberty/Verilog/LEF collateral, with automated termination/equalization selection and TX/RX co-optimization. Multi-PDK support (TSMC 16/65 nm, GF 45 nm) enables exploration across technology and packaging dimensions in minutes.

Key results show that package-level decisions dramatically impact PPA: organic substrates unexpectedly outperform silicon interposers at longer reaches (\sim 10 mm+). Future work extends to higher data rates where inductance matters and adds 3D chiplet support.

References

- [1] Jingwei Cai, Zuocong Wu, Sen Peng, Yuchen Wei, Zhanhong Tan, Guiming Shi, Mingyu Gao, and Kaisheng Ma. 2024. Gemini: Mapping and Architecture Co-exploration for Large-scale DNN Chiplet Accelerators. In *2024 IEEE International Symposium on High-Performance Computer Architecture (HPCA)*. 156–171. doi:10.1109/HPCA57654.2024.00022
- [2] UCIe Consortium. 2024. Universal Chiplet Interconnect Express (UCIe) 2.0 Specification.
- [3] Behzad Dehlaghi, Nijwm Wary, and Tony Chan Carusone. 2019. Ultra-Short-Reach Interconnects for Die-to-Die Links: Global Bandwidth Demands in Microcosm. *IEEE Solid-State Circuits Magazine* 11, 2 (2019), 42–53. doi:10.1109/MSSC.2019.2910619
- [4] Yinxiao Feng and Kaisheng Ma. 2022. Chiplet Actuary: a Quantitative Cost Model and Multi-Chiplet Architecture Exploration. In *Proceedings of the 59th ACM/IEEE Design Automation Conference (San Francisco, California) (DAC '22)*. Association for Computing Machinery, New York, NY, USA, 121–126. doi:10.1145/3489517.3530428

- [5] Yinxiao Feng, Dong Xiang, and Kaisheng Ma. 2023. Heterogeneous Die-to-Die Interfaces: Enabling More Flexible Chiplet Interconnection Systems. In *Proceedings of the 56th Annual IEEE/ACM International Symposium on Microarchitecture* (Toronto, ON, Canada) (*MICRO '23*). Association for Computing Machinery, New York, NY, USA, 930–943. doi:10.1145/3613424.3614310
- [6] Sandeep Goyal, Ganpat Parulekar, and Shalabh Gupta. 2022. A True Full-Duplex IO (TFD-IO) With Background SI Cancellation for High-Density Interfaces. *IEEE Transactions on Very Large Scale Integration (VLSI) Systems* 30, 5 (2022), 615–624. doi:10.1109/TVLSI.2022.3146326
- [7] Alexander Graening, Saptadeep Pal, and Puneet Gupta. 2023. Chiplets: How small is too small?. In *2023 60th ACM/IEEE Design Automation Conference (DAC)*. IEEE, 1–6.
- [8] Durand Jarrett-Amor, Kunal Yadav, Danny Zhang, Bangda Yang, Sadegh Jalali, and Tony Chan Carusone. 2023. A 32 Gb/s, 0.42 pJ/bit Passive Hybrid Simultaneous Bidirectional Transceiver for Die-to-Die Links. In *2023 IEEE International Symposium on Circuits and Systems (ISCAS)*. 1–5. doi:10.1109/ISCAS46773.2023.10181991
- [9] Durand Jarrett-Amor, Kunal Yadav, Danny Zhang, Bangda Yang, Sadegh Jalali, and Tony Chan Carusone. 2023. A 32 Gb/s, 0.42 pJ/bit Passive Hybrid Simultaneous Bidirectional Transceiver for Die-to-Die Links. In *2023 IEEE International Symposium on Circuits and Systems (ISCAS)*. 1–5. doi:10.1109/ISCAS46773.2023.10181991
- [10] Joohye Kim, Jun So Pak, Jonghyun Cho, Eakhwan Song, Jeonghyeon Cho, Heegon Kim, Taigon Song, Junho Lee, Hyungdong Lee, Kunwoo Park, et al. 2011. High-frequency scalable electrical model and analysis of a through silicon via (TSV). *IEEE Transactions on Components, Packaging and Manufacturing Technology* 1, 2 (2011), 181–195.
- [11] Kahyun Kim, Jung-Hun Park, Ha-Jung Park, Jia Park, Jihee Kim, and Woo-Seok Choi. 2025. 22.1 A 0.275pJ/b 42Gb/s/pin Clock-Referenced PAM3 Transceiver Tolerant to Supply Noise, Reference Offset and Crosstalk for Chiplets and Short-Reach Memory Interfaces. In *2025 IEEE International Solid-State Circuits Conference (ISSCC)*, Vol. 68. 394–396. doi:10.1109/ISSCC49661.2025.10904729
- [12] M. Lee, A. Singh, H.M. Torun, J. Kim, S. Lim, M. Swaminathan, and S. Mukhopadhyay. 2018. Automated Generation of All-Digital I/O Library Cells for System-in-Package Integration of Multiple Dies. In *2018 IEEE 27th Conference on Electrical Performance of Electronic Packaging and Systems (EPEPS)*. 65–67. doi:10.1109/EPEPS.2018.8534223
- [13] Zixi Li and David Wentzlaff. 2024. LUCIE: A Universal Chiplet-Interposer Design Framework for Plug-and-Play Integration. In *2024 57th IEEE/ACM International Symposium on Microarchitecture (MICRO)*. 423–436. doi:10.1109/MICRO61859.2024.00039
- [14] Susnata Mondal, Sashank Krishnamurthy, Shuhei Yamada, Zhaokai Liu, Junyi Qiu, Soumya Bose, Zuoguo Wu, Gerald Pasdast, James Jaussi, and Mozghan Mansuri. 2026. A 48Gb/s/lane 1.24Tb/s/mm UCle-Compliant Die-to-Die Link Over 30mm Standard Package. In *2026 IEEE International Solid-State Circuits Conference (ISSCC)*, Vol. 69. 134–136. doi:10.1109/ISSCC49663.2026.11409120
- [15] Lukas Pfromm, Alish Kanani, Harsh Sharma, Parth Solanki, Eric Tervo, Jaehyun Park, Janardhan Doppa, Partha Pratim Pande, and Umit Ogras. 2025. MFIT: Multi-Fidelity Thermal Modeling for 2.5D and 3D Multi-Chiplet Architectures. *ACM Trans. Des. Autom. Electron. Syst.* 31, 1, Article 4 (Nov. 2025), 27 pages. doi:10.1145/3765905
- [16] John W. Poulton, John M. Wilson, Walker J. Turner, Brian Zimmer, Xi Chen, Sudhir S. Kudva, Sanquan Song, Stephen G. Tell, Nikola Nedovic, Wenxu Zhao, Sunil R. Sudhakaran, C. Thomas Gray, and William J. Dally. 2019. A 1.17-pJ/b, 25-Gb/s/pin Ground-Referenced Single-Ended Serial Link for Off- and On-Package Communication Using a Process- and Temperature-Adaptive Voltage Regulator. *IEEE Journal of Solid-State Circuits* 54, 1 (2019), 43–54. doi:10.1109/JSSC.2018.2875092
- [17] Mirko Scholz, Geert Hellings, Shih-Hung Chen, Dimitri Linten, Mikael Detalle, Cesar Roda Neve, A. Shibkov, Antonio La Manna, Geert van der Plas, and Eric Beyne. 2015. ESD protection design in active-lite interposer for 2.5 and 3D systems-in-package. In *2015 37th Electrical Overstress/Electrostatic Discharge Symposium (EOS/ESD)*. 1–10. doi:10.1109/EOSED.2015.7314774
- [18] Zhanhong Tan, Hongyu Cai, Runpei Dong, and Kaisheng Ma. 2021. NN-Baton: DNN Workload Orchestration and Chiplet Granularity Exploration for Multi-chip Accelerators. In *2021 ACM/IEEE 48th Annual International Symposium on Computer Architecture (ISCA)*. 1013–1026. doi:10.1109/ISCA52012.2021.00083
- [19] Rao R. Tummala et al. 2001. Fundamentals of microsystems packaging. (2001).
- [20] Zhenyu Wang, Pragnya Sudershan Nalla, Jingbo Sun, A Alper Goksoy, Sumit K Mandal, Jae-sun Seo, Vidya A Chhabria, Jeff Zhang, Chaitali Chakrabarti, Umit Y Ogras, et al. 2025. HISIM: Analytical Performance Modeling and Design Space Exploration of 2.5 D/3D Integration for AI Computing. *IEEE Transactions on Computer-Aided Design of Integrated Circuits and Systems* (2025).
- [21] S.L. Wright, R. Polastre, H. Gan, L.P. Buchwalter, R. Horton, P.S. Andry, E. Sprogis, C. Patel, C. Tsang, J. Knickerbocker, J.R. Lloyd, A. Sharma, and M.S. Sri-Jayantha. 2006. Characterization of micro-bump C4 interconnects for Si-carrier SOP applications. In *56th Electronic Components and Technology Conference 2006*. 8 pp.–. doi:10.1109/ECTC.2006.1645716
- [22] Yang Zhang, Xuchen Zhang, and Muhannad S Bakir. 2018. Benchmarking digital die-to-die channels in 2.5-D and 3-D heterogeneous integration platforms. *IEEE Transactions on Electron Devices* 65, 12 (2018), 5460–5467.
- [23] Minghao Zhou, Li Li, Fengze Hou, Guoqiang He, and Jiaqi Fan. 2022. Thermal Modeling of a Chiplet-Based Packaging With a 2.5-D Through-Silicon Via Interposer. *IEEE Transactions on Components, Packaging and Manufacturing Technology* 12, 6 (2022), 956–963. doi:10.1109/TCPMT.2022.3174608